Redox Biology 84 (2025) 103658

Contents lists available at ScienceDirect

Redox Biology

journal homepage: www.elsevier.com/locate/redox

Interaction between 1-Cys peroxiredoxin and ascorbate in the response to H_2O_2 exposure in *Pseudomonas aeruginosa*

Rogerio L. Aleixo-Silva [a], Renato M. Domingos [a], Madia Trujillo [b], Fernando Gomes [a], Luciene O. Machado [c], Cristiano L.P. Oliveira [c], Regina Baldini [d], Luis E.S. Netto [a,*]

[a] From the Departamento de Genética e Biologia Evolutiva, Instituto de Biociências, Universidade de São Paulo, Brazil
[b] Departamento de Bioquímica, Facultad de Medicina y Centro de Investigaciones Biomédicas, Universidad de la República, Uruguay
[c] Instituto de Física, Universidade de São Paulo, Brazil
[d] Departamento de Bioquímica, Instituto de Química, Universidade de São Paulo, Brazil

ARTICLE INFO

Keywords:
H_2O_2 response
1-Cys peroxiredoxin
Pseudomonas aeruginosa, sulfenic acid
Ascorbate
LsfA

ABSTRACT

Pseudomonas aeruginosa, a leading cause of hospital-acquired infections, triggers host defenses, including oxidant release by phagocytes. Targeting bacterial antioxidants could reduce pathogen infectivity. This study investigates LsfA, a 1-Cys peroxiredoxin (Prx), member of the Prx6 subfamily, involved in *P. aeruginosa* virulence. LsfA efficiently reduced various peroxides (10^6-10^7 $M^{-1}s^{-1}$), while exhibiting hyperoxidation resistance ($k_{hyperoxidation}$ ~10^2 $M^{-1}s^{-1}$). Despite its substrate oxidizing promiscuity, LsfA displayed specific reduction by ascorbate (2.2 × 10^3 $M^{-1}s^{-1}$). Moreover, elucidating the LsfA's crystallographic structures in the reduced and sulfinic/sulfonic acid states at 2.4 and 2.0 Å resolutions unveiled possible residues related to ascorbate binding. Small-angle X-ray scattering (SAXS) and size-exclusion chromatography (SEC) confirmed LsfA as a dimer regardless of its oxidative state. Microbiological assays, including a real-time analysis employing Hyper7, a genetically encoded probe, showed that ascorbate enhanced H_2O_2 removal in a LsfA-dependent manner. Hence, our integrated structural, biochemical, and microbiological analyses underscored the significance of the ascorbate–LsfA pathway in *P. aeruginosa* response to H_2O_2.

1. Introduction

Pseudomonas aeruginosa, a gamma-proteobacteria, is a leading cause of nosocomial infections, as in burn wounds and cystic fibrosis cases [1,2], presenting the capacity to acquire multidrug resistance [3,4]. Host defenses against pathogens involve the action of phagocytes, which can release reactive oxygen (ROS), nitrogen (RNS), and chlorine species [5–8]. In response to these oxidative insults, *P. aeruginosa* employs a diverse array of antioxidant proteins, including peroxiredoxins (Prxs) [9].

Prxs are widespread and abundant thiol-based peroxidases [10], classified into six subgroups based on their amino acid sequences and structures [11]. These enzymes operate through either 1-Cys or 2-Cys mechanisms, according to the number of Cys residues involved in catalysis [12]. Despite these differences, all the Prxs share an N-terminal cysteine, known as peroxidatic cysteine (C_P) that takes part in a universal PxxxT/SxxC$_P$ motif. An arginine residue together with the T/S and C_P of the universal motif composes the catalytic triad that is fully conserved among all Prxs [13].

In all Prxs, the thiolate of C_P reduces peroxides through an S_N2 nucleophilic displacement mechanism, leading to the formation of a sulfenic acid (C_P –SOH) [14].While the initial oxidation step is similar in all Prxs, the mechanism for recycling C_P thiolate varies. In the case of 1-Cys Prxs, the identities of the reductants vary with the particular enzyme [15–19].Alternatively, C_P–SOH can undergo further oxidation, generating sulfinic acid (C_P–SO_2H) or even sulfonic acid (C_P–SO_3H). While C_P- SO_2H can be reduced in certain 2-Cys Prxs (from the Prx1/AhpC sub-group) by sulfiredoxin, no equivalent reductive system has been described so far in 1-Cys Prxs belonging to the Prx6 sub-group [20,21].

Some Prxs are implicated in pathogenesis [22], including AhpC (a 2-Cys Prx) and LsfA (a 1-Cys Prx) from *P. aeruginosa* [23,24]. Due to limited biochemical and structural information on bacterial 1-Cys Prxs, particularly those in the Prx6 sub-group, this study focuses on LsfA, a 1-Cys Prx that protects *P. aeruginosa* against oxidants derived from macrophages [24]. Therefore, this work aims: (i) to elucidate

* Corresponding author.
E-mail address: nettoles@ib.usp.br (L.E.S. Netto).

https://doi.org/10.1016/j.redox.2025.103658
Received 19 March 2025; Received in revised form 28 April 2025; Accepted 1 May 2025
Available online 8 May 2025

mechanisms by which LsfA protects *P. aeruginosa* from oxidants, (ii) to identify how LsfA is recycled to its reduced state, and (iii) provide structural insights to guide future searches for potential inhibitors.

In this regard, this study presents the first two *P. aeruginosa* Prx crystal structures, one in reduced (C_P–S^-) and the other in a mixture of sulfinic acid (C_P–SO_2H) and sulfonic acid (C_P–SO_3H) states, at 2.4 and 2.0 Å resolution, respectively. As other Prx6-type enzymes, LsfA exists as dimers across various oxidative states. With a robust reactivity toward multiple peroxides ($k_{oxidation}$ in the 10^6–10^7 M^{-1} s^{-1} range), LsfA demonstrated resilience against hyperoxidation ($k_{hyperoxidation}$ ~10^2 M^{-1} s^{-1}). Notably, LsfA was specifically reduced by ascorbate instead of thiol-based systems, with computational simulations pinpointing some residues that may be involved in enzyme-substrate interaction. Furthermore, utilizing a genetically encoded probe (Hyper7), our investigation underscores the role of the ascorbate-LsfA axis in the response of *P. aeruginosa* to H_2O_2.

2. Results

2.1. LsfA reduces with high efficiency a wide range of hydroperoxides

To gain evidence which oxidants LsfA protects the bacteria against, we evaluated its specificity by testing various peroxides. We first examined the reaction between reduced LsfA and peroxynitrite by the HRP competition assay [25]. As expected, increasing amounts of LsfA inhibited compound I formation (Fig. 1A), yielding a rate constant of (2.2 ± 0.4) x10^7 M^{-1} s^{-1} (Table 1). In addition to calculating the fractional inhibition, we also analyzed the data from Fig. 1A using the global fitting method [26], which yielded a similar rate constant (~2 × 10^7 M^{-1} s^{-1}) (Fig. S1). As a second independent approach, we assessed the initial rate of peroxynitrite decay at increasing LsfA concentrations (Fig. 1B) [27], yielding a rate constant of (1.9 ± 0.5) x10^7 M^{-1} s^{-1} at pH 7.4 and 25 °C (Table 1).

The reaction between reduced LsfA and H_2O_2 was also investigated by the HRP competition assay [25]. Again, at a fixed HRP concentration (2 μM), increasing amounts of LsfA inhibited HRP compound I generation (Fig. 1C). Again, the data analyzed by the fractional inhibition and by the global fitting [26] provided similar rate constants (~2 × 10^7 M^{-1} s^{-1}) (Fig. S1). Furthermore, we characterized this reaction by assessing redox-dependent changes in the intrinsic fluorescence of LsfA. Two phases were detected: an initial rapid decay followed by a subsequent gradual fluorescence increase (Fig. 1D). The k_{obs} values were determined by fitting the first phase to first exponential decays, which were dependent on H_2O_2 concentration (Fig. 1D, insert). These k_{obs} values were attributed to the oxidation step, as previously outlined for other Prxs [28–32]. Lastly, in a third independent approach, we employed a competition assay between H_2O_2 and peroxynitrite for LsfA [33,34], (Fig. 1E). Of note, the rate constant for the reaction between reduced LsfA with H_2O_2 determined by three independent assays yielded values around 3 × 10^7 M^{-1} s^{-1} (Table 1).

Regarding the second phase of the fluorimetric profile (Fig. 1F), k_{obs} values were obtained by fitting the experimental data to exponential increases, which were dose-dependent at H_2O_2 concentrations higher than 50 μM. The linear fit of the last yielded a slope that corresponds to the rate constant of hyperoxidation (302 ± 7) $M^{-1}s^{-1}$ at pH 7.4 and 25 °C (Fig. S2 and Table 1). Noteworthy, hyperoxidation of C_P was confirmed by western blotting (Fig. S3). At this point, we do not understand the phenomenon that resulted in the changes in k_{obs} being independent of H_2O_2 concentrations up to 50 μM (Fig. S2 and Supplementary text).

We also examined the oxidation of LsfA by an organic hydroperoxide (*tert*-butyl hydroperoxide, *t*-BOOH). We explored this reaction by the competition between peroxynitrite and *t*-BOOH for LsfA (Fig. 1G) and by the fluorimetric assay, following an approach similar to the one described for the oxidation of LsfA by H_2O_2 (Fig. 1H). By both assays, the rate constants were in the 10^6 M^{-1} s^{-1} range, one order of magnitude slower than the oxidations of LsfA by H_2O_2 and peroxynitrite (Table 1). The second-order rate constant for the hyperoxidation of LsfA by *t*-BOOH was also determined (Fig. 1I) and again confirmed by western blotting (Fig. S3).

Table 1 summarizes all the data regarding the oxidation and hyperoxidation of LsfA obtained herein. The $k_{oxidation}/k_{hyperoxidation}$ ratio was around 10^5 for H_2O_2 and 10^4 for *t*-BOOH. For comparison, human Prx2, Prx3 and AhpE from *Mycobacterium tuberculosis* display a $k_{oxidation}/k_{hyperoxidation}$ ratio of approximately 10^3 [35,36]. Similarly, Prx6 from *Plasmodium falciparum* (PfPrx6) has a $k_{oxidation}/k_{hyperoxidation}$ ratio of 10^5 and 10^3 for H_2O_2 and *t*-BOOH, respectively [30]. Although data regarding Prx hyperoxidation remain limited, these findings suggest that Prx6 enzymes (mostly 1-Cys Prx) are generally resistant to hyperoxidation. These data are consistent with the possibility of LsfA's potential to protect *P. aeruginosa* from various oxidants generated by the macrophages. This protective role likely arises not only from LsfA's high reactivity toward diverse oxidants but also from its notable resistance to hyperoxidation. Therefore, the kinetic properties of LsfA appear well-suited to support bacterial survival under condition of oxidative stress generated by phagocytic cells [7].

2.1.1. LsfA is specifically reduced by ascorbate

After establishing that LsfA exhibits broad substrate specificity toward oxidants, we investigated its reductive pathway. Previously, we described that LsfA is reduced by ascorbate with a rate constant in the 10^3 M^{-1} s^{-1} range at pH 7.2 and 25 °C [19]. Here, we described the expression and purification of different thiol-based systems from *P. aeruginosa* to assess their capacity to reduce LsfA. Initially, we showed that the reconstituted thioredoxin-dependent system efficiently reduced 5,5′-dithiobis (2-nitrobenzoic acid) (DTNB), an artificial disulfide substrate (Fig. S4). Then, using a standard coupled assay, we found that thioredoxin reductase B2 (PA14_53290), together with thioredoxin (Trx (PA14_11340) or TrxA (PA14_69200) failed to support LsfA peroxidase activity (Fig. S5 A and B). Likewise, no LsfA peroxidase activity was observed in the presence of glutathione alone or in combination with monothiolic glutaredoxin (PA14_18650) and glutathione reductase (Fig. S5 C).

As LsfA exhibited significant resistance to the reduction by distinct thiol-based systems (Fig. S5), ascorbate remained as the only reducing substrate described so far [19]. We cannot exclude, however, that other reductants might also support the peroxidase activity of LsfA.

This resistance to reduction by thiol-based systems is not unique to LsfA. For instance, Prx2 from *Toxoplasma gondii* is not reduced by GSH, Grx or Trx [37]; Prx6 from *Arenicola marina* is resistant to reduction by both H_2S and thioredoxin [33]; and *Plasmodium falciparum* Prx1 is not reduced by several other reductants, in this case including also ascorbate [38,39]. In contrast, wheat PER1 can be reduced by both ascorbate and Trx [19,40]; yeast Prx1 is reduced by ascorbate, thioredoxin 3, and GSH/Grx2 [18,19,41], and mammalian Prx6 is reduced by glutathione/glutathione transferase, H_2S, dihydrolipoic acid, and ascorbate [19,42–44]. These examples highlight the heterogeneity of reductant preferences within the Prx6 subgroup.

2.1.2. Structural insights into LsfA from P. aeruginosa

We elucidated two crystallographic structures in reduced (C_P–S^-, PDB_{id} = 6P0W) and a mixture of sulfinic and sulfonic acid (PDB_{id} = 7KUU) states, achieving 2.4 and 2.0 Å resolutions, respectively (Fig. 2). These structures provide valuable insights into the substrate specificity of LsfA. Regarding the 7KUU crystal structure, the analysis of the 2mFo-DFc map at 1 rmsd (blue map) indicated C_P in the sulfinic acid state (Fig. S6A), while the mFo-DF map at 3.0 rmsd (green map) revealed the presence of the third oxygen (Fig. S6B), indicating that LsfA also adopted the sulfonic acid state. These are the first reported structures of Prxs from *P. aeruginosa*. The two LsfA structures form antiparallel dimers (Fig. 2A), exhibiting the typical arrangement for proteins belonging to the Prx6 subgroup (type B dimer) and displaying the characteristic

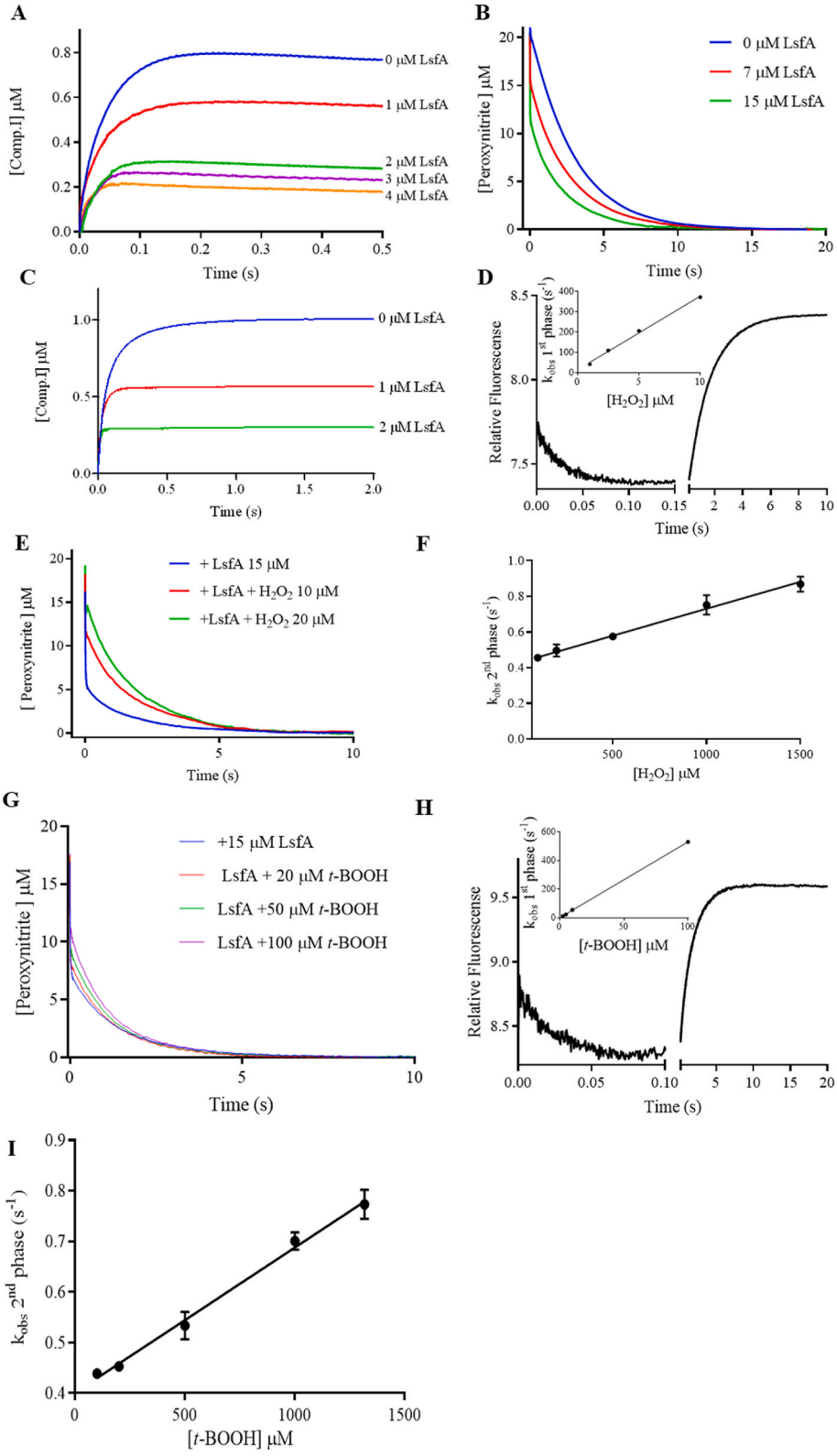

(caption on next page)

Fig. 1. Kinetics of LsfA oxidation by various peroxides. A) HRP competition assay, using HRP (5 μM), peroxynitrite (1 μM), and increasing concentrations of LsfA (0–4 μM). B) Peroxynitrite decay assay performed with a fixed concentration of peroxynitrite (20 μM), while varying LsfA concentrations (0–15 μM). C) HRP competition assay with fixed concentrations of HRP (2 μM) and H_2O_2 (0.91 μM), while increasing concentrations of LsfA (0–2 μM). D) Redox-dependent changes on the intrinsic fluorescence of LsfA (1 μM) were followed upon H_2O_2 treatment (1 μM). The curves of the first phase were fitted with first-order exponential functions to obtain the observed rate constants k_{obs}. Inset: Plot of k_{obs} versus H_2O_2 concentration, where the slope represents the second-order rate constant. E) Peroxides competition assay, using fixed concentrations of peroxynitrite (20 μM) and LsfA (15 μM)and increasing H_2O_2 concentrations (0, 10 and 20 μM). Reactions were monitored by the absorbance decay of peroxynitrite. F) Determination of k_{obs} by fitting first-order exponential functions to the second phase of reactions containing LsfA (1 μM) and increasing H_2O_2 concentrations (100–1500 μM). An illustrative experiment is depicted in panel D. G) Peroxynitrite competition assay using a fixed concentration of peroxynitrite (20 μM) and LsfA (15 μM) and varying *t*-BOOH concentration. H) Redox-dependent changes in the intrinsic fluorescence of LsfA (1 μM) followed upon *t*-BOOH treatment (100 μM). The initial phase was fitted with a first-order exponential to obtain *kobs*. Inset: Plot of *kobs* versus *t*-BOOH concentration, where the slope represents the second-order rate constant. I) k_{obs} were obtained by fitting first-order exponential functions to the second phase of reactions containing LsfA (1 μM) and increasing *t*-BOOH concentrations (100–1500 μM).

Table 1
Summary of all rate constants determined in this work with LsfA, indicating oxidant, method and the resulting constant. Further details in the text.

Oxidant	Method	Second order constant rate ($M^{-1}.s^{-1}$)
Oxidation		
H_2O_2	HRP competition	$2.2 \pm 0.6 \times 10^7$
	Intrinsic Fluorescence	$3.6 \pm 0.2 \times 10^7$
	Peroxynitrite Decay	$3.3 \pm 0.6 \times 10^7$
***t*-BOOH**	Intrinsic Fluorescence	$0.2 \pm 0.04 \times 10^7$
	Peroxynitrite Decay	$0.1 \pm 0.04 \times 10^7$
Peroxynitrite	HRP competition	$2.2 \pm 0.4 \times 10^7$
	Peroxynitrite Decay	$1.9 \pm 0.5 \times 10^7$
Hyperoxidation		
H_2O_2	Intrinsic Fluorescence	302.3 ± 7
***t*-BOOH**	Intrinsic Fluorescence	286.9 ± 11.3

thioredoxin fold (Fig. 2B) [13]. The overall shapes of the two structures are highly similar (Fig. 2A), differing only in the active site (Fig. 2C and D).

In both cases, aside from the fully conserved catalytic triad (Thr42; C_P; Arg122), His 37 is positioned close to C_P within α helix 5, (Fig. 2C and D), a typical feature of Prx6-type enzymes. The oligomerization of LsfA in the native, reduced, oxidized and hyperoxidized states is always dimeric, as determined by SAXS analyses and size exclusion chromatography (Figs. S7 and S8). The indirect Fourier transform (IFT) modeling curves for all samples are similar, indicating that the treatments did not lead to important changes in the protein structure (Fig. S8). The obtained P(r) curve revealed an overall maximum size of ~65 Å, indicating a globular shape, corroborating with the radius of gyration and molecular weight (Table S1).

Other members of the Prx6 subfamily exhibit similar behavior. For instance, Prx2 from *Toxoplasma gondii* is dimeric in both oxidized and reduced states [37] and Prx1 from *Saccharomyces cerevisiae* is dimeric under native conditions [41]. Mammalian Prx6 is also mostly dimeric, although it can form high molecular weight oligomers when hyperoxidized [42]. Similarly, Prx6 from *Arenicola marina* forms covalent dimers in its oxidized state and even tetramers in a crystallographic structure [45]. In contrast, Prx1 from *Plasmodium falciparum* exhibits a monomer/dimer equilibrium [38], while Prx6 from *Aeropyrum pernix* K1 displays hexadecameric oligomerization [46].

A search on the Protein Data Bank - PDB (https://www.rcsb.org/), using DALI server (http://ekhidna2.biocenter.helsinki.fi/dali/) and LsfA (6P0W) as a template [47], returned structures of nine different proteins, all belonging to the Prx6 subgroup. These Prx6 enzymes share high amino acid sequence similarity (Fig. S9), mainly at the PVCTTE motif [11]. As expected, the overall structures of Prx6 enzymes are highly similar, each featuring a hydrophobic patch surrounding their active sites adjacent to the C_P (Fig. S10). Notably, the electrostatic surfaces around the active sites differ among the analyzed Prx6s in the reduced state (Fig. 3A). Specifically, LsfA (6P0W), TkPrx (6IU0), PhPrx (3W6G) and ApPrx (3A5W) display a highly positively charged surface near their active sites, while HsPrx6 (5B6M) shows only a weak positive charge in this region. These structural variations may indicate differing affinities for substrates and/or inhibitors.

An investigation into the LsfA active site revealed a close interaction between C_P and His37 in both structures (6P0W and 7KUU). His37 is highly conserved among Prx6 members, and its interaction with C_P was highlighted before through the description of a hypervalent state [48]. In *Anabaena* sp., the conserved His residue was described as presenting high mobility [49]. Accordingly, in HsPrx6 the positions occupied by this His residue are dependent on the oxidative state [50]. Comparing the available Prx6 structures in the reduced state, we observed that the side chain of His37 in LsfA (6P0W) was the only one positioned in a distinct configuration (Fig. 3B and C). In contrast, His 37 in one of LsfA's structures (7KUU) presented a similar configuration to His residues of the other Prx6 structures (Fig. 3C). Finally, it was recently proposed that this conserved His residue would protect C_P from hyperoxidation [38], which is consistent with the high $k_{oxidation}/k_{hyperoxidation}$ described here for LsfA (Table 1).

We also sought to gain structural insights into the interaction between LsfA and ascorbate, which is currently the only known biological reducing substrate for this enzyme. After unsuccessful attempts to co-crystalize LsfA and ascorbate, we turned to unbiased computer simulations. These simulations revealed that ascorbate docked into the LsfA active site (Fig. S11A), aligning with the positively charged surface near the active site (Fig. 3A). The calculated binding energy for the LsfA–ascorbate complex was relatively low ($\Delta G = -4.2$ kcal/mol), suggesting a transient interaction characteristic of enzyme-substrate complexes, where reversible binding often precedes catalysis. Notably, the carbon 2 of ascorbate is positioned in the direction of the gamma sulfur atom of C_P (Fig. S11A), consistent with the reaction mechanism proposed for the reduction of sulfenic acids by this reductant [51,52].

A recurrent interaction was observed between the Thr120 residue and ascorbate through hydrogen bonding. Additionally, hydrophobic interactions were also observed, involving Pro38, Thr42, Pro43, Val44, and Arg122 (the catalytic arginine) residues (Fig. S11B and C). Notably, the interactions involving Pro38, Pro43, and Val44 are conserved in two other proteins from the Prx6 subfamily (Fig. S12). This conservation suggests that these residues play a role in facilitating the interaction with ascorbate.

2.1.3. Cellular assays

The roles of LsfA in the *P. aeruginosa* response to oxidative insults were investigated by assessing the phenotypes of Δ*lsfA*, a strain whose *lsfA* gene was deleted [24]. Following incubation with 3-ATZ (a catalase inhibitor), the Δ*lsfA* strain exhibited heightened sensitivity compared to the wild-type (WT) strain when exposed to paraquat, a compound that generates a flux of H_2O_2 through spontaneous superoxide dismutation (Fig. 4A). Additionally, the Δ*lsfA* strain was significantly more susceptible to bolus addition of H_2O_2 (Fig. 4B) as previously described [24]. Moreover, the Δ*lsfA* strain appeared to be more sensitive to SIN-1 (a peroxynitrite generator) compared to the WT strain (Fig. 4A), although this result did not achieve statistical significance. Noteworthy, other bacterial peroxidases, such as Ohr [9], can reduce peroxynitrite with similar efficiency. Surprisingly, Δ*lsfA* strain exhibited increased resistance to *t*-BOOH (Fig. 4B). This unexpected result might be attributable

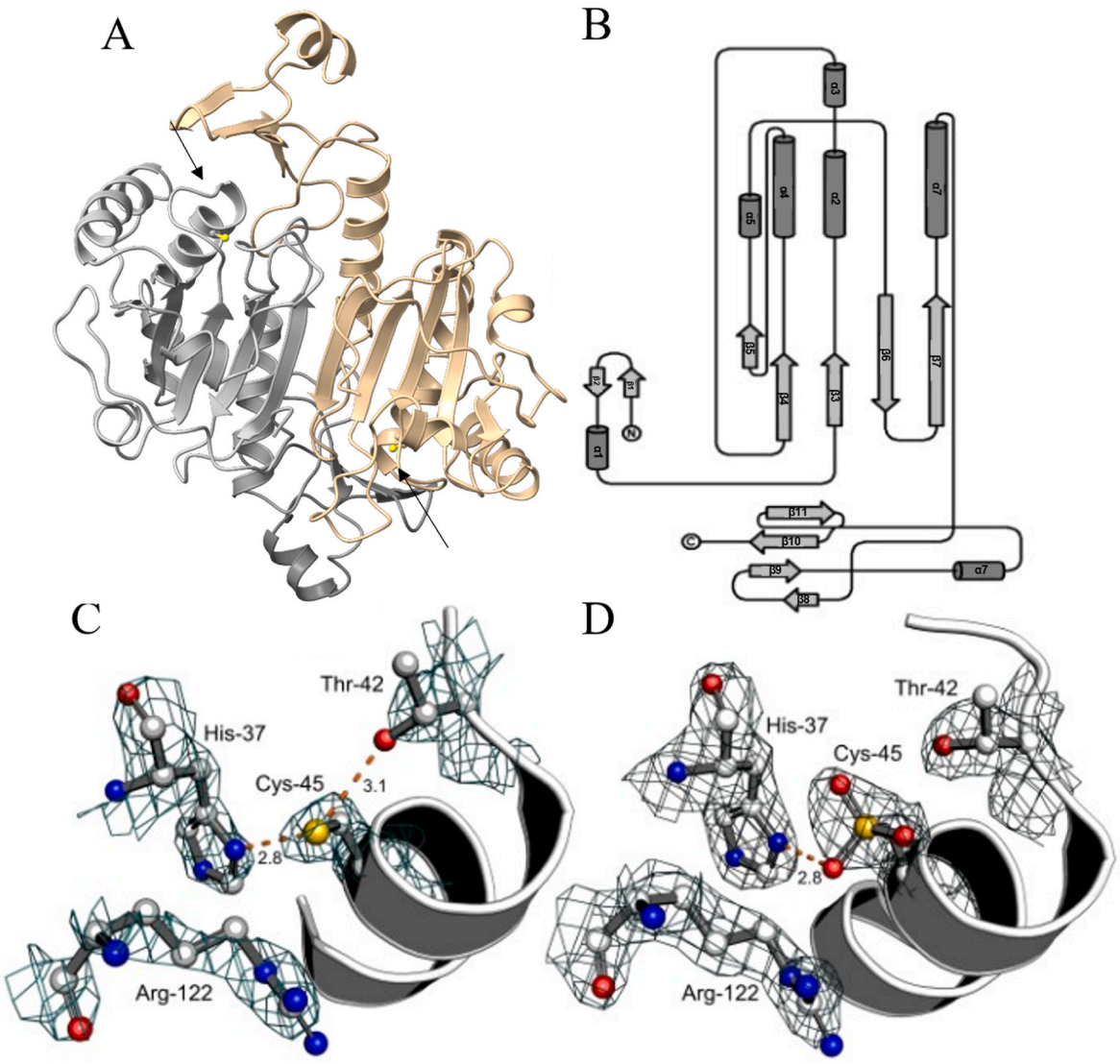

Fig. 2. Structural characterization of LsfA. A) Crystallographic structure of reduced LsfA (PDB ID: 6P0W), showing the characteristic β -strand dimerization interface. One subunit of the dimer is colored in copper and the other is shown in gray. The active site, containing the C_P, is indicated by the black arrows. B) Secondary-structure topology of LsfA, highlighting the arrangement of α-helices and β-strands, with the active site located at the N-terminal region of α-helix 2. C) Close-up view of the active site of reduced LsfA (PDB ID: 6P0W), with C_P shown within 2Fo-Fc electron density map. D) Close-up view of the active site of LsfA in the sulfonic acid state (PDB ID: 7KUU), also displayed with its corresponding 2Fo-Fc electron density map. Both electron density maps were contoured at 1.5 σ units in PyMOL. For additional details regarding electron density maps, please refer to Fig. S6.

to a compensatory effect, possibly involving the induction of one of the several peroxidases in *P. aeruginosa*. Compensatory effects among antioxidant systems are well-documented and can lead to mutant strains more resistant to oxidants than the wild-type counterparts [53–55].

Utilizing the Hyper7 probe [56], the H_2O_2 levels were monitored in real-time, without disrupting the cellular compartmentalization. Of note, this is the first study employing genetically encoded probes in *P. aeruginosa*. We first confirmed the expression of Hyper7 in *P. aeruginosa,* followed by an assessment of the response of both strains harboring the empty vector, which showed no response (Fig. S13). Following exposure to H_2O_2, the Hyper7 signal was consistently higher in the Δ*lsfA* strain than in the WT for all tested concentrations, consistent with the notion that LsfA outcompeted Hyper7 for H_2O_2 reduction in the wild-type strain (Fig. 4C and D). Additionally, the recovery of the Hyper7 fluorescence to the basal state was delayed in the Δ*lsfA* strain (Fig. 4C and D). Collectively, these findings indicated that LsfA plays a major role in the response of *P. aeruginosa* to H_2O_2.

Given the limited information available on ascorbate metabolism in *P. aeruginosa,* we investigated its involvement in the bacterial response to H_2O_2. As *E. coli* and *Vibrio cholerae* can use ascorbate as a sole carbon source [57,58], we explored whether *P. aeruginosa* could exhibit a similar capability. However, at high ascorbate concentrations, we observed only minimal bacterial growth when this molecule was used as the sole carbon source (Fig. S14). Subsequently, we verified that ascorbate (up to 10 mM) did not impair bacterial growth in a M9 media containing glucose (Fig. S15).

Finally, we investigated whether ascorbate could enhance the peroxidase activity of LsfA in cellular systems, taking advantage of Hyper7 [56]. In this regard, redox-dependent changes in Hyper7 fluorescence were monitored in WT (Fig. 5A and C) or Δ*lsfA* (Fig. 5B and D), and the cells were exposed to 4 mM H_2O_2 (first dotted line) followed by ascorbate (second dotted line). Remarkably, ascorbate accelerated the recovery of Hyper7 fluorescence only in WT (Fig. 5A and C), while no such effect was observed in Δ*lsfA* strain (Fig. 5B and D). This data supports the notion that *P. aeruginosa* can internalize ascorbate and use it to support LsfA peroxidase activity.

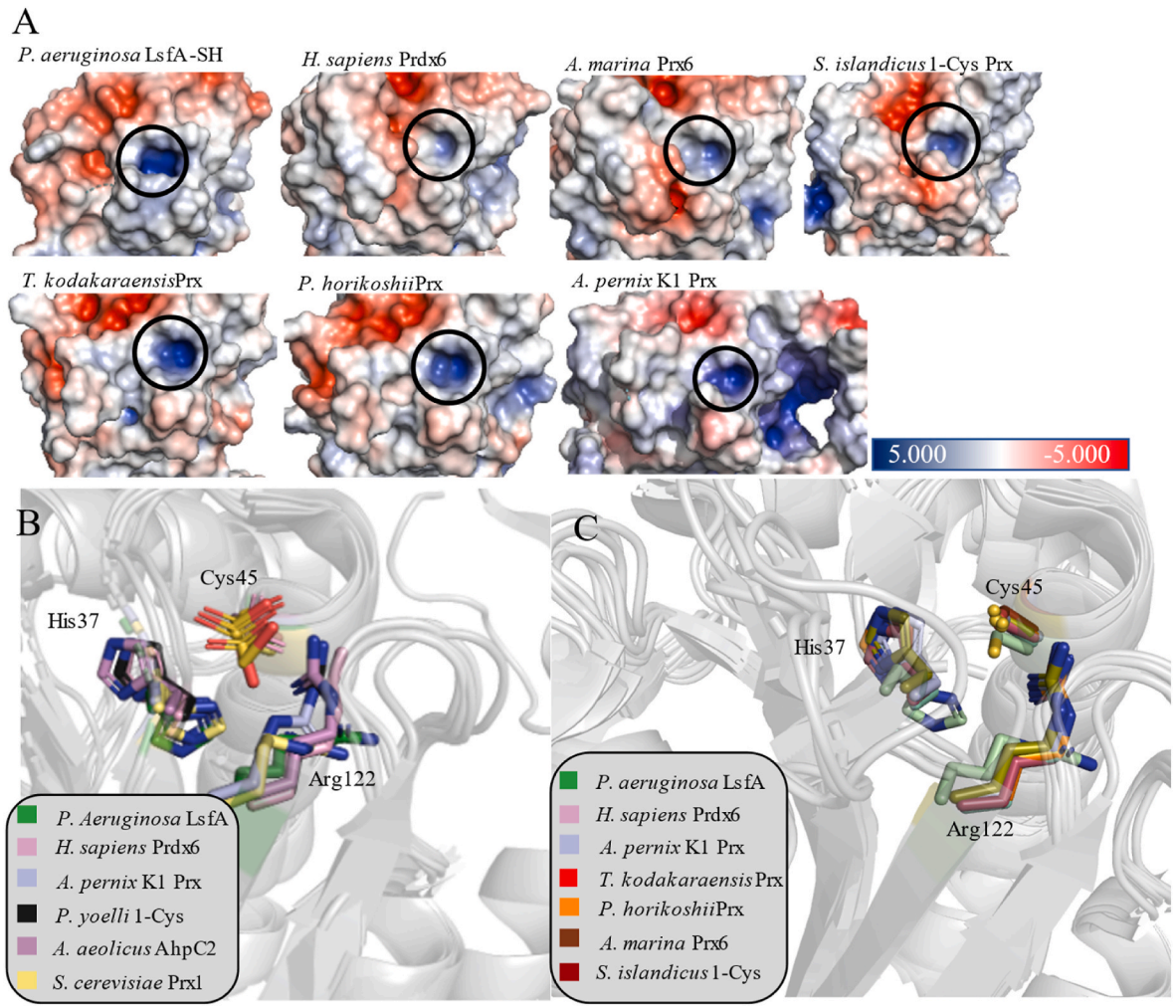

Fig. 3. Structural comparison among Prx6 family members. A) Electrostatic surface representation of one subunit from each Prx6 structure. Blue color indicates positively charged areas, while red regions represent negatively charged areas. The black circle highlights the positively charged active site. B) and C) Superposition of the active sites from different Prx6-type of enzymes, emphasizing the highly mobile His residue, the conserved arginine and C_P in either reduced or (hyper) oxidized, respectively. The PDB codes are as follow: *P. aeruginosa* LsfA (7KUU and 6P0W), *Homo sapiens* Prdx6 (5B6M and 5B6N), *Saccharomyces cerevisiae* Prx1 (5YKJ), *Arenicola marina* Prx6 (2V2G), *Aquifex aeolicus* AhpC2 (5OVQ), *Plasmodium yoelli* 1-Cys (3TB2), *Sulfolobus islandicus* 1-Cys Prx (6Q5V), *Thermococcus kodakaraensis* Prx (6IU0), *Aeropyrum pernix* K1 Prx (2E2M and 3A5W) and *Pyrococcus horikoshii* Prx (3W6G).

3. Discussion

LsfA is implicated with *P. aeruginosa* virulence as evidenced in macrophages and mouse models, defending bacteria against oxidants derived from NOX2 of macrophages [24]. Therefore, gaining insights into the molecular aspects related to LsfA function may provide valuable information regarding host-pathogen interactions. *P. aeruginosa* presents a large number of antioxidant proteins capable of decomposing hydroperoxides [23], indicating a complex response to oxidants, which tend to specialize in removing specific types of hydroperoxides. For instance, Ohr is related to bacterial protection against fatty acid hydroperoxides and peroxynitrite [9]. Consequently, a compensatory effect involving the upregulation of another peroxidase may explain the enhanced resistance of Δ*lsfA* strain towards *t*-BOOH (Fig. 4B).

Regarding the *P. aeruginosa* response to H_2O_2, evidence indicated that LsfA plays a central role [24]. Indeed, Δ*lsfA* strain exhibited heightened sensitivity to H_2O_2 (Fig. 4A and B) and an impaired ability to reduce H_2O_2 (Fig. 4C and D). Furthermore, recombinant LsfA displayed extraordinary efficiency in reducing H_2O_2, with a rate constant of 3×10^7 M^{-1}. s^{-1} (Fig. 1C, D, and E). Additionally, LsfA expression is up-regulated by paraquat, a compound well known to generate a H_2O_2 flux through superoxide dismutation [59–61]. Moreover, the transcription factor OxyR, which orchestrates the *P. aeruginosa* response to H_2O_2 [62], has been found to bind to the LsfA promoter region [63].

Our data also highlighted the role of ascorbate in *P. aeruginosa's* response to H_2O_2, which is dependent on LsfA (Fig. 5). We previously described that ascorbate can reduce sulfenic acids in 1-Cys Prxs [19,64]. Here, we provide structural evidence that ascorbate can interact in the active site of LsfA and other 1-Cys Prx enzymes through hydrophobic interactions and hydrogen bonds (Figs. S11 and S12). These structural analyses are consistent with the mechanism proposed by You et al. [51], in which the enolate form at carbon 2 of ascorbate attacks the gamma sulfur atom of C_P sulfenic acid (C_P–SOH), forming a covalent intermediate. Subsequently, the sulfur atom accepts electrons from ascorbate, resulting in the formation of dehydroascorbic acid and the regeneration of the enzyme's thiol group (R–SH), as further illustrated in the book chapter by Conte and Carroll [52].

However, evidence for ascorbate as a reducing substrate for Prx enzymes in biological systems is scarce [65]. In the case of *P. aeruginosa*, information on ascorbate metabolism is limited [66], and there are currently no identified genes associated with its biosynthesis. However, our findings demonstrate that ascorbate can penetrate the bacterial cytoplasm and act as an intracellular reductant (Fig. 5). This suggests that *P. aeruginosa* may uptake ascorbate from immune cells, such as

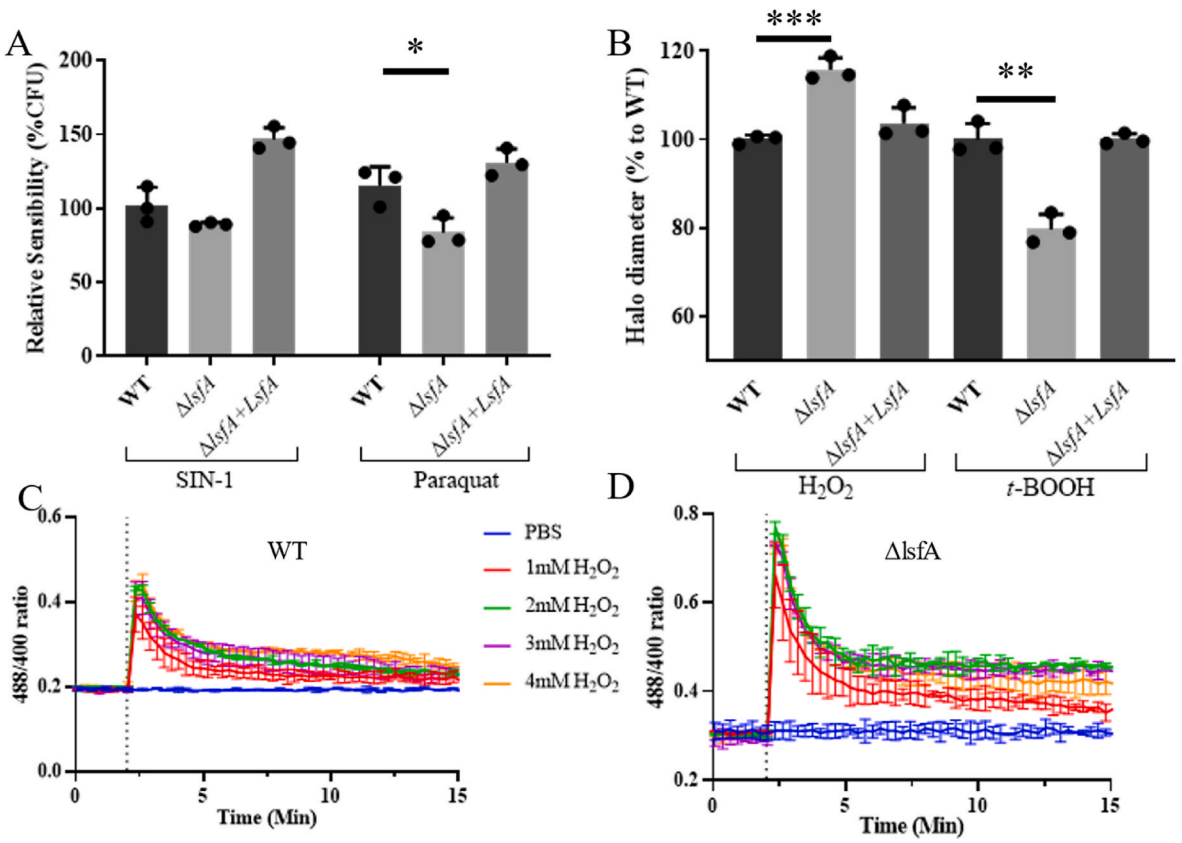

Fig. 4. Roles of LsfA in the response of P. aeruginosa to oxidative insults. A) Wild type (WT), Δ*lsfA* or Δ*lsfA* complemented with LsfA (Δ*lsfA* + LsfA) strains were treated with 3 mM SIN-1 or 2.5 mM paraquat, for 30 min at 37 °C. Prior to treatment, cells were pre-incubated with 5 mM ATZ for 10 min, to inhibit catalase activity. Survival was determined by counting colony-forming units (CFUs) after 16 h at 37 °C, where data are expressed as the percentage of CFU relative to untreated controls (n = 3, *p < 0.05 by unpaired *t*-test). Untreated cells presented around 50 to 100 colonies after a one million times dilution. B) Halo inhibition assay. A filter disk containing either 2 % H_2O_2 or 1 % t-BOOH was placed on solid culture plates seeded with WT, Δ*lsfA* or Δ*lsfA* + LsfA strains. After 16 h of incubation at 37 °C, the diameter of the halo was measured. Data are expressed as the percentage relative to treated WT strain (n = 3, **p < 0.0020, ***p = 0.0006 by unpaired *t*-test). The halo distances for WT and Δ*lsfA* treated with H_2O_2 were around 1 cm for the WT and 1.2 cm for the ΔlsfA. C and D) Oxidation ratio of Hyper7 probe expressed in WT (C) or in Δ*lsfA* (D) in OD = 7 in PBS at 37 °C, at increasing H_2O_2 concentrations as depicted in the legend. Results are expressed by a representative experiment of a biological replicate (n = 3) and as means of technical duplicates (n = 2).

lymphocytes, monocytes, and neutrophils, where concentrations can reach millimolar levels [67].

An important cautionary note concerns the reduction of Hyper7 in *P. aeruginosa*, which is expected to follow similar principles to those observed in human cells, where the probe was originally validated. In human cells, Hyper7 is predominantly reduced by the Grx/GSH system, and a similar mechanism is likely operative in *P. aeruginosa*. However, the experiments presented in Figs. 4 and 5 are comparative in nature, and thus baseline differences in the reducing systems are not expected to significantly affect Hyper7 fluorescence interpretation. Nevertheless, the potential influence of the Grx/GSH system in *P. aeruginosa* warrants further investigation to fully validate and interpret the Hyper7 signal in this organism.

Ascorbate is known to inhibit *P. aeruginosa* quorum sensing and biofilm formation, reduce pyocyanin production, and enhance motility at concentrations ranging from 2 to 68 mM [68–70]. These processes are closely linked to the virulence of this bacterium. Our results indicated that ascorbate enhances the ability of *P. aeruginosa* to reduce H_2O_2 in an LsfA-dependent manner. Therefore, LsfA and ascorbate are two molecules involved in *P. aeruginosa* virulence and may operate in the same pathway of the bacterial response to H_2O_2.

In the context of bacterial virulence, it is notable that while the LsfA and Prdx6 structures are overall similar, their electronic surface properties differ considerably (Fig. 3A). These distinctions may provide opportunities for developing specific inhibitors targeting the bacterial enzyme, potentially paving the way for novel therapeutic strategies.

4. Experimental procedures

4.1. Cloning, expression, and purification of recombinant protein

LsfA gene was cloned into expression vector pET15b (Novagen, Madison, USA) within the *Nde*I and *Bam*HI restriction sites, using the following primers: LsfA: 5′-CGCAT**CATATG**CTCAGACTCGGCGAC-3′ and 5′-AC**GGATCC**TCAGCGGTTGGGCTG-3′. *E. coli* BL21 (*DE3*) was transformed with the pET15b- *LsfA* gene. For *LsfA* expression, single colonies were cultured in LB broth supplemented with 100 μg/mL ampicillin and grown for 16 h at 37° C in an orbital shaker (250 rpm). The culture was then diluted in 0.75 L of LB (100 μg/mL ampicillin) and incubated at 30° C until the optical density (OD_{600nm}) attained 0.6–0.8 values. Isopropyl *β*-D-1-thiogalactopyranoside (IPTG) was added to a final concentration of 0.5 mM, followed by an additional 6-h incubation at 30 °C (250 rpm). Cells were harvested by centrifugation, and the pellet was washed and resuspended in 20 mM sodium phosphate pH 7.4; 500 mM NaCl. Cell suspensions underwent twenty cycles of sonication (15 s at 30 % amplitude followed by 45 s on ice). The suspension was then centrifuged at 15 000 rpm for 45 min to remove nucleic acid precipitates and the insoluble fraction. Finally, the cell extract was filtered. Filtered cell extracts were purified by immobilized metal ion affinity chromatography (IMAC) by the HisTrap™ FF 5 mL column (GE

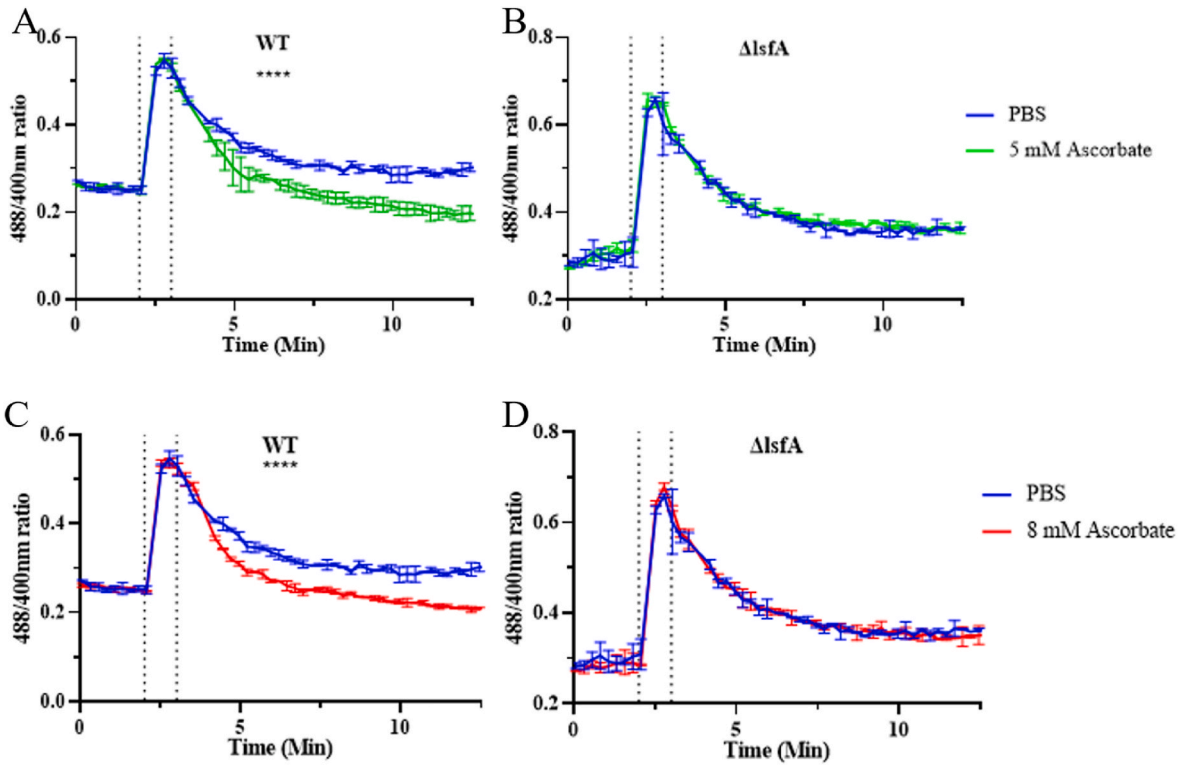

Fig. 5. Capacity of *P. aeruginosa* to use ascorbate for supporting H_2O_2 removal in a LsfA dependent manner. Oxidation ratio of Hyper7 probe expressed in WT (A and C) or Δ*lsfA* (B and D) at an OD = 7 in PBS at 37 °C. The first dotted line indicates the addition of 4 mM of H_2O_2, while the second dotted line, 1 min later, marks the addition of either PBS (blue line) or ascorbate (5 mM in green or 8 mM in red line). Results are presented as a representative experiment of biological replicates (n = 3) and as the mean of technical duplicates. Mann-Whitney test showed a highly significant difference between PBS and ascorbate in WT strains ****p < 0.0001, while no significant difference were observed in Δ*lsfA* strains.

Healthcare, Chicago, USA) on the ÄKTA FPLC system (GE Healthcare, Chicago, USA). Protein purification conditions were optimized using the gradient procedure for imidazole concentration as described by the manufacturer. Imidazole was removed from purified protein using a PD10 column through gel filtration (GE Healthcare, Chicago, USA). Final protein buffer consisted of 20 mM HEPES buffer (pH 7.4) containing 150 mM NaCl and 0.1 mM diethylenetriaminepentaacetic acid (DTPA). Recombinant protein concentration was determined spectrophotometrically at 280 nm, using the corresponding extinction coefficients for reduced protein (E_{280nm} = 33 920 M^{-1} cm^{-1}) determined using the ProtPram tool (http://www.expasy.ch/tools/protparam.html, Lausanne, Switzerland).

4.1.1. Reduction of proteins and quantification of their sulfhydryl groups

LsfA was treated with a 20-fold excess of dithiothreitol (DTT) for 30 min at room temperature. Excess of DTT was removed using two coupled HiTrap Desalting Columns (GE Healthcare). The number of reduced thiols in LsfA was determined spectrophotometrically by the reaction with 4,4′-dithiodipyridine [71].

4.1.2. Kinetic analyses

The HRP competitive assay was used to characterize the reaction between reduced LsfA with H_2O_2 or with peroxynitrite [25]. *In this* competition method, H_2O_2 or peroxynitrite can react either with HRP or with LsfA, following the formation of HRP Compound I at 398 nm ($\varepsilon_{398\ nm}$ = 42 000 $M^{-1}cm^{-1}$), which is the isosbestic point between Compound I and Compound II. This is important as Compound I decays rapidly to Compound II. Given the fast kinetics of these reactions, we used the stopped flow apparatus from Applied Photophysics SX20, which has a mixing time of less than 2 ms [28]. The assay was conducted at a fixed HRP concentration (2 μM for H_2O_2 experiments and 5 μM for peroxynitrite experiments), H_2O_2/peroxynitrite (1 μM), and varying LsfA concentrations at 25 °C in 100 mM $NaHPO_4$ buffer supplemented with 0.1 mM DTPA at pH 7.4. Each point was measured at least five times, with at least two independent experiments. In addition to the commonly used fractional inhibition method, the recently proposed global fitting approach was also performed to calculate the rate constants between LsfA and the peroxides [26], using Dynafit program version 4.11.073 (dated September 29, 2023) [72].

Redox-dependent changes in the intrinsic fluorescence changes of LsfA were investigated using an excitation wavelength of 280 nm and registering total emission at >320 nm (using an emission filter) [28]. Reduced LsfA (1 μM) was mixed with oxidant in varying concentrations, as indicated in the text. The observed rate constants for both oxidation and hyperoxidation (k_{obs}) values were determined by fitting the first and second phase of the reaction to a single exponential equation, respectively. The second-order constants rate were obtained from the slope of the plot k_{obs} versus oxidant concentration. All assays were conducted at 11.5 °C in 100 mM $NaHPO_4$ at pH 7,4 buffer supplemented with DTPA 0, 1 mM. The rates reported here represent averages from at least five measurements per oxidant concentration, performed in duplicate.

Peroxynitrite reduction by reduced LsfA was investigated by a direct approach, monitoring the rapid peroxynitrite decay at 310 nm (ε: 1600 M^{-1} cm^{-1}) in a SX-17 Applied Photophysics stopped-flow spectrophotometer. Taking advantage of the determined rate constant between peroxynitrite and LsfA, we conducted an additional assay: the competition between peroxynitrite and other hydroperoxides for LsfA as described in Ref. [27], while continuing to monitor peroxynitrite decay. These assays were carried out in 100 mM $NaHPO_4$ buffer at pH 7,4 supplemented with DTPA 0,1 mM buffer. Peroxynitrite solutions were freshly prepared daily in 10 mM NaOH at 25 °C. A fixed peroxynitrite concentration (20 μM) was used alongside varying LsfA concentrations, as described in the text.

4.1.3. Western blotting

To assess hyperoxidation, recombinant LsfA (0.5 mg) that was previously incubated overnight at 4°C with different concentrations of oxidants was loaded in an SDS-PAGE and the gel was subsequently electroblotted onto a 0.45 μm nitrocellulose membrane, which was blocked for 1 h at room temperature in Tris-buffered saline (TBS) containing 0.1 % Tween-20 (TBS-T) and 5 % (vol/wt) nonfat dry milk (Bio-Rad). Then, the membrane was probed with a rabbit anti-PrxVI SO3 (AbFrontier LF-0005) at a 1:2000 dilution in (TBS-T) supplemented with 5 % (vol/wt) nonfat dry milk for 1 h at room temperature, followed by a thorough wash with TBS-T. Subsequently, the membrane was incubated with Anti-rabbit IgG-HRP (cell signalling#7074S) at a 1:10000 TBST+5 % non-fat milk for 1 h at room temperature and washed again with TBS-T. Protein bands were visualized with the ECL™ prime Western blotting detection reagent (GE Health-care).

To assess Hyper7 expression, *P. aerginosa* cells harboring the pUCp18-Hyper7 plasmid or the corresponding empty vector were freshly transformed and grown overnight in LB media supplemented with 300 μg/mL carbenicillin. Cells were harvested using 5x Laemmli buffer and centrifuged at 16000×*g* at 4 °C for 10 min. Equivalent concentrations of total proteins were boiled at 95 °C in the presence of 50 mM DTT and separated by SDS-PAGE on a 14 % polyacrylamide gel. Following electrophoresis, proteins were transferred to a nitrocellulose membrane and labeled with anti-GFP, N-terminal antibody (Sigma, G1544) which recognizes the different GFP isoforms.

4.2. Structural characterization

4.2.1. Crystallization

Crystallization screening was conducted at the robotic facility of the Brazilian National Biosciences Laboratory, RoboLab. Crystals were grown using vapor diffusion (sitting drop) at 18 °C with a 20-fold excess of TCEP (Tris(2-carboxyethyl) phosphine hydrochloride). The structures were obtained from crystals grown under two different conditions [1]: phosphate citrate 0.1 M pH 5.5, Sodium Chloride 0.2 M and PEG 3000 10 %w/v for the reduced LsfA [2]; Sodium phosphate citrate 0.1 M pH 5.25, Sodium Chloride 0.2 M and PEG 8000 10 % w/v for the sulfinic/sulfonic acid forms. In both cases, LsfA concentration was 5.2 mg/mL.

4.2.2. Structure solution

The crystallographic data for the reduced form were collected at the Stanford Synchrotron Radiation Light source (SSRL) and processed with XDS [73]. Data collection for the sulfinic/sulfonic acid forms of LsfA was conducted at the MX2 beamline at the Brazilian Synchrotron Light Laboratory (LNLS), with subsequent processing utilizing autoPROC [62]. Molecular replacement was performed with MOLREP [63], utilizing the structure of Prx6 (PDB ID: 1PRX) as a template to solve the phase problem for the reduced LsfA structure (PDB ID: 6P0W). For the molecular replacement of the sulfonic acid LsfA structure (PDB ID: 7KUU), the reduced LsfA structure (PDB ID: 6P0W) was used as the template. Refinement of both structures was carried out using REFMAC 5 [64] and Coot [65], both of which are components of the CCP4 software suite [66], with manual verification performed using Coot. Unit cell parameters and data collection are shown in Table 2. The final resolution was selected due to the limitation of the other parameters in a higher resolution.

In both structures (PDB ID: 6P0W and 7KUU), we were unable to model the region between amino acids 111–119, consistent with a highly flexible segment in LsfA. This observation is supported by our molecular modeling analysis using the ARP/wARP software, which predicted increased mobility in this segment (data not shown).

4.2.3. Molecular Simulations

Molecular Simulations were conducted using the structures of reduced LsfA (PDB ID: 6P0W), Human Prx6 (PDB ID: 5B6M) or ScPrx1 (PDB ID: 5YKJ). For LsfA, we predicted the unresolved loop (amino acids 109–120) using ARP/wARP loop software [74]. The preparation of LsfA structure and of the ascorbate molecule were carried out using MGLTools (http://mgltools.scripps.edu/downloads), which involved removing water molecules, adding polar hydrogens, and computing Gasteiger charges. A grid box of 30x30 × 30 Å, centered on the C_P of one monomer was used for docking simulations. The AutoDock Vina software [64] was run with an exhaustiveness setting of 24, and the best 20 models were selected for analysis. The results were evaluated using ChimeraX software [65]. Interactions between the LsfA protein and ascorbate were visualized using ChimeraX.

Table 2
Crystallographic data from both solved structures generated using Phenix software (ADAMS et al., 2011).

	6P0W	7KUU
Resolution range	33.72 - 2.4 (2.486 - 2.4)	29.28 - 2.0 (2.071 - 2.0)
Space group	P 61 2 2	P 1 21 1
Unit cell	82.427 82.427 102.859 90 90 120	41.569 95.239 59.83 90 105.923 90
Total reflections	17104 (1664)	52766 (5568)
Unique reflections	8552 (832)	26581 (2568)
Multiplicity	2.0 (2.0)	2.0 (2.0)
Completeness (%)	99.92 (100.00)	86.26 (85.17)
Mean I/sigma(I)	11.57 (2.38)	11.42 (0.40)
Wilson B-factor	36.69	24.83
R-merg	0.0415 (0.3072)	0.05282 (3.08)
R-meas	0.0587 (0.4344)	0.0747 (4.356)
R-pim	0.0415 (0.3072)	0.05282 (3.08)
CC1/2	0.999 (0.851)	0.998 (0.864)
CC*	1 (0.959)	1 (0.963)
Reflections used in refinement	8551 (832)	26118 (2562)
Reflections used for R-free	440 (44)	1236 (124)
R-work	0.2175 (0.2867)	0.2171 (0.3896)
R-free	0.2833 (0.3457)	0.2546 (0.4141)
CC(work)	0.935 (0.638)	0.934 (0.454)
CC(free)	0.891 (0.415)	0.922 (0.352)
Number of non-hydrogen atoms	1649	3417
macromolecules	1622	3278
ligands	1	0
solvent	26	139
Protein residues	201	406
RMS(bonds)	18	14
RMS(angles)	1.91	1.87
Ramachandran favored (%)	97.46	97.7
Ramachandran allowed (%)	2.54	2.3
Ramachandran outliers (%)	0	0
Rotamer outliers (%)	9.39	3.86
Clashscore	7.1	4.9
Average B-factor	40.01	29.48
macromolecules	40.09	29.5
ligands	47.43	
solvent	34.84	29.04

4.2.4. SEC (size exclusion chromatography)

LsfA (4.2 mg/mL = 174 μM) was treated with a 20-fold excess of DTT or 100–fold excess of H_2O_2 to obtain the reduced or hyperoxidized samples, respectively. These samples were then subjected to an SEC-s2000 Phenomenex column and analyzed for 15 min using a PDA detector (280 nm) and a fluorescence detector (excitation: 280 nm, emission: 350 nm) in a Prominence –i LC 2060 Plus HPLC (Shimadzu). All the samples were analyzed in a HEPES 20 mM pH 7.4, NaCl 150 mM, DTPA 0.1 mM buffer.

4.2.5. SAXS (small angle x-ray scattering)

For SAXS analysis, LsfA (7.25 mg/mL = 300 μM) was studied in its native state and also treated with a 20-fold excess of DTT to obtain the

reduced sample. For the oxidized protein (Cys-SOH), reduced LsfA was treated with equimolar amounts of H_2O_2. For the hyperoxidized (Cys – $S_{2/3}OH$) sample, reduced LsfA was treated with a 10-fold excess of H_2O_2. The data acquisition was performed at the Multiuser SAXS Center EMUSAXS with Xenocs-XEUSS 2.0 system. For the data acquisition, 6 frames of 1800s were collected. The programs used for analysis were Fit2D, SUPERSAXS, IFT, and CRYSOL [75–78]. The PDB structure 7KUU was used as a model for the comparison.

4.2.6. Cellular assays

Disk diffusion (Halo) assay.

This assay was conducted as outlined in Ref. [24]. Briefly, overnight cultures of WT, Δ*lsfA* or Δ*lsfA* + LsfA strains (*P. aeruginosa* PA14 harboring empty PJN105 or with lsfA) in LB broth plus 50 μg/mL gentamycin and 0.2 % of L-arabinose. Cultures were diluted to $O.D._{600nm}$ = 0.1 and grown until $O.D._{600nm}$ = 1. Subsequently, 3 mL of 0.7 % soft LB agar was poured into petri dishes containing LB medium, and 200 μL of bacterial culture was spread evenly onto the agar. Sterile paper disks (~6 mm diameter), three per plate, were saturated with 2.5 % H_2O_2 or 1 % t-BOOH that were placed on the plate and incubated for 16 h at 37 °C. Following incubation, plates were photographed, and the diameters of the inhibition zones (haloes) were measured using imageJ software. Experiments conducted in triplicates.

4.2.7. Colony counting assay

The assay was performed as described before [9]. Briefly, bacterial strains were grown in LB broth supplemented with 50 μg/mL gentamycin and 0.2 % of L-arabinose at 37 °C until reaching an $O.D._{600nm}$ = 1. The cultures were then washed twice with PBS and diluted to an $O.D._{600nm}$ = 0.1. Next, 200 μL of cell suspension was treated with 5 mM aminotriazol (ATZ) for 10 min at room temperature. Then, either 3 mM SIN-1 or 2.5 mM paraquat was added and cells were incubated for 30 min at 37 °C. Treated cells were serially diluted in 10 mM $MgSO_4$ and plated on solid LB broth, and the colony formation units (CFU) were assessed after 16 h at 37 °C. The results were expressed as a percentage relative to untreated cells. All experiments were performed at least three biological replicates.

4.2.8. Hyper7 oxidation detection

PA14 WT or Δ*lsfA* strains constitutively expressing Hyper 7 (pUC-p18Hyper7) were grown overnight in LB medium supplemented 300 μg/mL carbenicillin. Then, cells were washed twice with PBS and diluted in PBS to an $O.D._{600nm}$ of 7. Fluorescence measurements were measured using a black plate with a flat clear bottom in a Synergy H1(BioTek® Instruments, Inc.) at two excitation wavelengths (400 and 488 nm) and 520 nm as the emission wavelength, as described in Ref. [79]. To assess the bacterial response to H_2O_2, the fluorescence emission ratio (488nm/400 nm) baseline was measured for 2 min, then H_2O_2 (1–4 mM) was added, and the fluorescence ratio was followed. In some experiments, ascorbate (5 or 8 mM) was added 1 min after H_2O_2 addition. The normality of the data was checked using the Shapiro-Wilk test, indicating non-normality, in this way, the Mann-Whitney test was used to compare the whole curves of the strains treated with PBS or ascorbate.

Classification

Biological Sciences, Biochemistry.

CRediT authorship contribution statement

Rogerio L. Aleixo-Silva: Writing – review & editing, Writing – original draft, Validation, Methodology, Investigation, Formal analysis, Data curation, Conceptualization. **Renato M. Domingos:** Visualization, Validation, Methodology, Investigation, Formal analysis, Data curation. **Madia Trujillo:** Writing – review & editing, Methodology, Investigation, Formal analysis, Data curation, Conceptualization. **Fernando Gomes:** Methodology, Investigation, Formal analysis, Data curation. **Luciene O. Machado:** Investigation, Formal analysis. **Cristiano L.P. Oliveira:** Investigation, Formal analysis. **Regina Baldini:** Writing – review & editing, Writing – original draft, Methodology, Formal analysis. **Luis E.S. Netto:** Writing – review & editing, Writing – original draft, Supervision, Project administration, Methodology, Investigation, Funding acquisition, Formal analysis, Data curation, Conceptualization.

Declaration of competing interest

The authors declare that they have no known competing financial interests or personal relationships that could have appeared to influence the work reported in this paper.

Acknowledgements

This work was financially supported by Fundação de Amparo á Pesquisa do Estado de São Paulo (FAPESP) Grant 13/07937-8 (Redox Processes in Biomedicine) (to L.E.S.N.) and by Universidad de la República, Uruguay (CSIC i + d 2020) and PEDECIBA, Programa de Desarrollo de Ciencias Básicas, Uruguay (to M.T). R. L. A. S. (2018/157752-6 and 2020/00845-4) was recipient of fellowships from Conselho Nacional de Desenvolvimento Científico e Tecnológico (CNPq) and FAPESP; R. M. D. was recipient of fellowships from CNPq and Coordenação de Aperfeiçoamento de Pessoal de Nível Superior (CAPES). We also thank Dr. Bruce Morgan (Saarland University, Germany) for discussions related to the Hyper7 probe and Dr. Patrick M. Dansette (Directeur de Recherche Emérite au CNRS, France) for insightful discussions on the mechanism of sulfenic acid reduction by ascorbate.

Appendix A. Supplementary data

Supplementary data to this article can be found online at https://doi.org/10.1016/j.redox.2025.103658.

Data availability

Data will be made available on request.

References

[1] M. Chatterjee, et al., Antibiotic resistance in Pseudomonas aeruginosa and alternative therapeutic options, Int. J. Med. Microbiol. 306 (2016) 48–58.
[2] N. Mesaros, et al., Pseudomonas aeruginosa: resistance and therapeutic options at the dawn of the 2d millennium, Antibiotiques 9 (2007) 189–198.
[3] D. Yordanov, T. Strateva, Pseudomonas aeruginosa – a phenomenon of bacterial resistance, J. Med. Microbiol. 58 (2009) 1133–1148.
[4] S. Harbarth, et al., Global priority list of antibiotic-resistant bacteria to guide research, discovery, and development of new antibiotics. http://www.who.int/medicines/publications/WHO-PPL-Short_Summary_25Feb-ET_NM_WHO.pdf?ua=1, 2017.
[5] T.A. Missall, J.K. Lodge, J.E. McEwen, Mechanisms of resistance to oxidative and nitrosative stress: implications for fungal survival in mammalian hosts, Eukaryot. Cell 3 (2004) 835–846.
[6] C. Nathan, M.U. Shiloh, Reactive oxygen and nitrogen intermediates in the relationship between mammalian hosts and microbial pathogens, Proc. Natl. Acad. Sci. 97 (2000) 8841–8848.
[7] C.C. Winterbourn, A.J. Kettle, M.B. Hampton, Reactive oxygen species and neutrophil function, Annu. Rev. Biochem. 85 (2016) 765–792.
[8] L. Piacenza, A. Zeida, M. Trujillo, R. Radi, The superoxide radical switch in the biology of nitric oxide and peroxynitrite, Physiol. Rev. 102 (2022) 1881–1906.
[9] T.G.P. Alegria, et al., Ohr plays a central role in bacterial responses against fatty acid hydroperoxides and peroxynitrite, Proc. Natl. Acad. Sci. 114 (2017) E132–E141.
[10] M. Trujillo, C.A. Tairum, M.A. de Oliveira, L.E.S. Netto, Thiol- and Selenol-Based Peroxidases: Structure and Catalytic Properties, Elsevier Inc., 2022, https://doi.org/10.1016/B978-0-323-90219-9.00008-X.
[11] K.J. Nelson, et al., Analysis of the peroxiredoxin family: using active-site structure and sequence information for global classification and residue analysis, Proteins: Struct., Funct., Bioinf. 79 (2011) 947–964.
[12] S.G. Rhee, S.W. Kang, T.S. Chang, W. Jeong, K. Kim, Peroxiredoxin, a novel family of peroxidases, IUBMB Life 52 (2001) 35–41.

[13] A. Hall, K. Nelson, L.B. Poole, P.A. Karplus, Structure-based insights into the catalytic power and conformational dexterity of peroxiredoxins, Antioxidants Redox Signal. 15 (2011) 795–815.

[14] A. Zeida, et al., The extraordinary catalytic ability of peroxiredoxins: a combined experimental and QM/MM study on the fast thiol oxidation step, Chem. Commun. 50 (2014) 10070–10073.

[15] A. Perkins, K.J. Nelson, D. Parsonage, L.B. Poole, P.A. Karplus, Peroxiredoxins: guardians against oxidative stress and modulators of peroxide signaling, Trends Biochem. Sci. 40 (2015) 435–445.

[16] G. Monteiro, B.B. Horta, D.C. Pimenta, O. Augusto, L.E.S. Netto, Reduction of 1-Cys peroxiredoxins by ascorbate changes the thiol-specific antioxidant paradigm, revealing another function of vitamin C, Proc. Natl. Acad. Sci. U. S. A 104 (2007) 4886–4891.

[17] A.B. Fisher, Peroxiredoxin 6: a bifunctional enzyme with glutathione peroxidase and phospholipase A $_2$ activities, Antioxidants Redox Signal. 15 (2011) 831–844.

[18] J.R. Pedrajas, A. Miranda-Vizuete, N. Javanmardy, J.Å. Gustafsson, G. Spyrou, Mitochondria of Saccharomyces cerevisiae contain one-conserved cysteine type peroxiredoxin with thioredoxin peroxidase activity, J. Biol. Chem. 275 (2000) 16296–16301.

[19] V. Anschau, et al., Reduction of sulfenic acids by ascorbate in proteins, connecting thiol-dependent to alternative redox pathways, Free Radic. Biol. Med. 156 (2020).

[20] A.W. Hyun, et al., Reduction of cysteine sulfinic acid by sulfiredoxin is specific to 2-Cys peroxiredoxins, J. Biol. Chem. 280 (2005) 3125–3128.

[21] S. Akter, et al., Chemical proteomics reveals new targets of cysteine sulfinic acid reductase, Nat. Chem. Biol. (2018), https://doi.org/10.1038/s41589-018-0116-2.

[22] M.A. de Oliveira, et al., Relevance of peroxiredoxins in pathogenic microorganisms, Appl. Microbiol. Biotechnol. 105 (2021) 5701–5717.

[23] L.S. Rocha, et al., Peroxiredoxin AhpC1 protects Pseudomonas aeruginosa against the inflammatory oxidative burst and confers virulence, Redox Biol. 46 (2021) 102075.

[24] G.H. Kaihami, et al., Involvement of a 1-cys peroxiredoxin in bacterial virulence, PLoS Pathog. 10 (2014).

[25] J.C. Toledo, et al., Horseradish peroxidase compound i as a tool to investigate reactive protein-cysteine residues: from quantification to kinetics, Free Radic. Biol. Med. 50 (2011) 1032–1038.

[26] C.J. Barry, C.S. Pillay, J.M. Rohwer, Direct fitting improves the accuracy of the horse radish peroxidase competition assay for peroxidase activity, Redox Biochem. Chem. 8 (2024) 100025.

[27] M. Trujillo, G. Ferrer-Sueta, R. Radi, Kinetic studies on peroxynitrite reduction by peroxiredoxins, Methods Enzymol. (2008) 173–196.

[28] M. Trujillo, et al., Pre-steady state kinetic characterization of human peroxiredoxin 5: taking advantage of Trp84 fluorescence increase upon oxidation, Arch. Biochem. Biophys. 467 (2007) 95–106.

[29] D. Parsonage, et al., Dissecting peroxiredoxin catalysis: separating binding, peroxidation, and resolution for a bacterial AhpC, Biochemistry 54 (2015) 1567–1575.

[30] K. Feld, et al., Tyrosine substitution of a conserved active-site histidine residue activates Plasmodium falciparum peroxiredoxin 6, Protein Sci. 28 (2019) 100–110.

[31] C.A. Tairum, et al., Catalytic Thr or ser residue modulates structural switches in 2-cys peroxiredoxin by distinct mechanisms, Sci. Rep. 6 (2016) 1–12.

[32] S. Portillo-Ledesma, et al., Differential kinetics of two-cysteine peroxiredoxin disulfide formation reveal a novel model for peroxide sensing, Biochemistry 57 (2018) 3416–3424.

[33] E. Loumaye, et al., Kinetic studies of peroxiredoxin 6 from Arenicola marina: rapid oxidation by hydrogen peroxide and peroxynitrite but lack of reduction by hydrogen sulfide, Arch. Biochem. Biophys. 514 (2011) 1–7.

[34] I.V. Peshenko, H. Shichi, Oxidation of active center cysteine of bovine 1-Cys peroxiredoxin to the cysteine sulfenic acid form by peroxide and peroxynitrite, Free Radic. Biol. Med. 31 (2001) 292–303.

[35] A.V. Peskin, et al., Hyperoxidation of peroxiredoxins 2 and 3: rate constants for the reactions of the sulfenic acid of the peroxidatic cysteine, J. Biol. Chem. 288 (2013) 14170–14177.

[36] A.M. Reyes, et al., Oxidizing substrate specificity of Mycobacterium tuberculosis alkyl hydroperoxide reductase E: kinetics and mechanisms of oxidation and overoxidation, Free Radic. Biol. Med. 51 (2011) 464–473.

[37] M. Deponte, K. Becker, Biochemical characterization of Toxoplasma gondii 1-Cys peroxiredoxin 2 with mechanistic similarities to typical 2-Cys Prx, Mol. Biochem. Parasitol. 140 (2005) 87–96.

[38] L. Lang, et al., Substrate promiscuity and hyperoxidation susceptibility as potential driving forces for the Co-evolution of prx5-type and prx6-type 1-cys peroxiredoxin mechanisms, ACS Catal. (2023) 3627–3643.

[39] C. Nickel, S. Rahlfs, M. Deponte, S. Koncarevic, K. Becker, Thioredoxin networks in the malarial parasite Plasmodium falciparum, Antioxidants Redox Signal. 8 (2006) 1227–1239.

[40] P. Pulido, R. Cazalis, F.J. Cejudo, An antioxidant redox system in the nucleus of wheat seed cells suffering oxidative stress, Plant J. 57 (2009) 132–145.

[41] J.R. Pedrajas, C.A. Padilla, B. McDonagh, J.A. Bárcena, Glutaredoxin participates in the reduction of peroxides by the mitochondrial 1-CYS peroxiredoxin in Saccharomyces cerevisiae, Antioxidants Redox Signal. 13 (2010) 249–258.

[42] Y. Manevich, S.I. Feinstein, A.B. Fisher, Activation of the antioxidant enzyme 1-CYS peroxiredoxin requires glutathionylation mediated by heterodimerization with GST, Proc. Natl. Acad. Sci. 101 (2004) 3780–3785.

[43] S. Shahnaj, et al., Hyperoxidation of peroxiredoxin 6 induces alteration from dimeric to oligomeric state, Antioxidants 8 (2019) 33.

[44] I. V Peshenko, H. Shichi, Oxidation of active center cysteine of bovine 1-Cys peroxiredoxin to the cysteine sulfenic acid form by peroxide and peroxynitrite, Free Radic. Biol. Med. 31 (2001) 292–303.

[45] A. Smeets, et al., The crystal structure of the C45S mutant of annelid Arenicola marina peroxiredoxin 6 supports its assignment to the mechanistically typical 2-Cys subfamily without any formation of toroid-shaped decamers, Protein Sci. 17 (2008) 700–710.

[46] S.J. Jeon, K. Ishikawa, Characterization of novel hexadecameric thioredoxin peroxidase from Aeropyrum pernix K1, J. Biol. Chem. 278 (2003) 24174–24180.

[47] L. Holm, L.M. Laakso, Dali server update, Nucleic Acids Res. 44 (2016) W351–W355.

[48] T. Nakamura, et al., Oxidation of archaeal peroxiredoxin involves a hypervalent sulfur intermediate, Proc. Natl. Acad. Sci. 105 (2008) 6238–6242.

[49] Y. Mishra, et al., Active-site plasticity revealed in the asymmetric dimer of AnPrx6 the 1-Cys peroxiredoxin and molecular chaperone from Anabaena sp. PCC 7210, Sci. Rep. 7 (2017) 17151.

[50] K.H. Kim, W. Lee, E.E.K. Kim, Crystal structures of human peroxiredoxin 6 in different oxidation states, Biochem. Biophys. Res. Commun. 477 (2016) 717–722.

[51] K.-S. You, L.V. Benitez, W.A. McConachie, W.S. Allison, The conversion of glyceraldehyde-3-phosphate dehyrogenase to an acylphosphatase by trinitroglycerin and inactivation of this activity by azide and ascorbate, Biochim. Biophys. Acta Enzymol. 384 (1975) 317–330.

[52] M. Lo Conte, K.S. Carroll, The chemistry of thiol oxidation and detection, in: Oxidative Stress and Redox Regulation, Springer Netherlands, 2013, pp. 1–42.

[53] K. Cosgrove, et al., Catalase (KatA) and alkyl hydroperoxide reductase (AhpC) have compensatory roles in peroxide stress resistance and are required for survival, persistence, and nasal colonization in Staphylococcus aureus, J. Bacteriol. 189 (2007) 1025–1035.

[54] D.C. Munhoz, L.E.S. Netto, Cytosolic thioredoxin peroxidase I and II are important defenses of yeast against organic hydroperoxide insult: catalases and peroxiredoxins cooperate in the decomposition of H2O2 by yeast, J. Biol. Chem. 279 (2004).

[55] R. Ogusucu, D. Rettori, D.C. Munhoz, L.E. Soares Netto, O. Augusto, Reactions of yeast thioredoxin peroxidases I and II with hydrogen peroxide and peroxynitrite: rate constants by competitive kinetics, Free Radic. Biol. Med. 42 (2007) 326–334.

[56] V.V. Pak, et al., Ultrasensitive genetically encoded indicator for hydrogen peroxide identifies roles for the oxidant in cell migration and mitochondrial function, Cell Metab. 31 (2020) 642–653.e6.

[57] Shan Yew Wen, J.A. Gerlt, Utilization of L-ascorbate by Escherichia coli K-12: assignments of functions to products of the yjf-sga and yia-sgb operons, J. Bacteriol. 184 (2002) 302–306.

[58] J.R. Rosenberger, N.D. McDonald, E.F. Boyd, L-ascorbic acid (vitamin C) fermentation by the human pathogen Vibrio cholerae</em&gt, bioRxiv 2020 (2020) 288738, 09.08.

[59] N.J. Hare, et al., Proteomics of the oxidative stress response induced by hydrogen peroxide and paraquat reveals a novel AhpC-like protein in Pseudomonas aeruginosa, Proteomics 11 (2011) 3056–3069.

[60] M. Palma, D. Deluca, S. Worgall, L.E.N. Quadri, Transcriptome analysis of the response of Pseudomonas aeruginosa to hydrogen peroxide 186 (2004) 248–252.

[61] D.A. Small, W. Chang, F. Toghrol, W.E. Bentley, Toxicogenomic analysis of sodium hypochlorite antimicrobial mechanisms in Pseudomonas aeruginosa, Appl. Microbiol. Biotechnol. 74 (2007) 176–185.

[62] U.A. Ochsner, M.L. Vasil, E. Alsabbagh, K. Parvatiyar, D.J. Hassett, Role of the Pseudomonas aeruginosa oxyR-recG operon in oxidative stress defense and DNA repair: OxyR-dependent regulation of katB-ankB, ahpB, and ahpC-ahpF, J. Bacteriol. 182 (2000) 4533–4544.

[63] Q. Wei, et al., Global regulation of gene expression by OxyR in an important human opportunistic pathogen, Nucleic Acids Res. 40 (2012) 4320–4333.

[64] G. Monteiro, B.B. Horta, D.C. Pimenta, O. Augusto, L.E.S. Netto, Reduction of 1-Cys peroxiredoxins by ascorbate changes the thiol-specific antioxidant paradigm, revealing another function of vitamin C, Proc. Natl. Acad. Sci. U. S. A 104 (2007) 4886–4891.

[65] E. Zito, H.G. Hansen, G.S.H. Yeo, J. Fujii, D. Ron, Endoplasmic reticulum thiol oxidase deficiency leads to ascorbic acid depletion and noncanonical scurvy in mice, Mol. Cell 48 (2012) 39–51.

[66] T.M.M. Stack, et al., Characterization of an l -ascorbate catabolic pathway with unprecedented enzymatic transformations, J. Am. Chem. Soc. 142 (2020) 1657–1661.

[67] A. Ang, J.M. Pullar, M.J. Currie, M.C.M. Vissers, Vitamin C and immune cell function in inflammation and cancer, Biochem. Soc. Trans. 46 (2018) 1147–1159.

[68] W.M. Abdelraheem, et al., Assessment of antibacterial and anti-biofilm effects of vitamin C against Pseudomonas aeruginosa clinical isolates, Front. Microbiol. 13 (2022) 1–9.

[69] T. Das, et al., Ascorbic acid modulates the structure of the Pseudomonas aeruginosa virulence factor pyocyanin and ascorbic acid-furanone-30 combination facilitate biofilm disruption, Front. Microbiol. 14 (2023).

[70] S.A. El-Mowafy, M.I. Shaaban, K.H. Abd El Galil, Sodium ascorbate as a quorum sensing inhibitor of Pseudomonas aeruginosa, J. Appl. Microbiol. 117 (2014) 1388–1399.

[71] D.R. Grassetti, J.F. Murray, Determination of sulfhydryl groups with 2,2'- or 4,4'-dithiodipyridine, Arch. Biochem. Biophys. 119 (1967) 41–49.

[72] P. Kuzmič, Program DYNAFIT for the analysis of enzyme kinetic data: application to HIV proteinase, Anal. Biochem. 237 (1996) 260–273.

[73] W. Kabsch, Xds. Acta Crystallogr. Sect. D Biol. Crystallogr. 66 (2010) 125–132.

[74] G. Langer, S.X. Cohen, V.S. Lamzin, A. Perrakis, Automated macromolecular model building for X-ray crystallography using ARP/wARP version 7, Nat. Protoc. 3 (2008) 1171–1179.
[75] A.P. Hammersley, FIT2D : a multi-purpose data reduction, analysis and visualization program, J. Appl. Crystallogr. 49 (2016) 646–652.
[76] C.L.P. Oliveira, T. Vorup-Jensen, C.B.F. Andersen, G.R. Andersen, J.S. Pedersen, in: M. Gomez, A. Nogales, M.C. Garcia-Gutierrez, T.A. Ezquerra (Eds.), Discovering New Features of Protein Complexes Structures by Small-Angle X-Ray Scattering, Springer Berlin Heidelberg, 2009.
[77] C.L.P. Oliveira, et al., A SAXS study of glucagon fibrillation, J. Mol. Biol. 387 (2009) 147–161.
[78] D. Svergun, C. Barberato, M.H.J. Koch, CRYSOL – a program to evaluate X-ray solution scattering of biological macromolecules from atomic coordinates, J. Appl. Crystallogr. 28 (1995) 768–773.
[79] P. Kritsiligkou, T.K. Shen, T.P. Dick, A comparison of Prx- and OxyR-based H2O2 probes expressed in S. cerevisiae, J. Biol. Chem. 297 (2021) 100866.